JCTC Journal of Chemical Theory and Computation

Computational and Spectroscopic Studies of Re(I) Bipyridyl Complexes Containing 2,6-Dimethylphenylisocyanide (CNx) Ligand

Stanislav R. Stoyanov,[†] John M. Villegas,[†] Arvin J. Cruz,[†] Loranelle L. Lockyear,[‡]
Joseph H. Reibenspies,[§] and D. Paul Rillema*,[†]

*Department of Chemistry, Wichita State University, 1845 N. Fairmount Street,
Wichita, Kansas 67260-0051, Department of Chemistry, Bethany College,
421 N. First Street, Lindsborg, Kansas 67456-1897, and Department of Chemistry,
Texas A & M University, P.O. Box 30012, College Station, Texas 77842-3012*

Abstract: Density Functional Theory (DFT) calculations produce optimized geometries of the complexes $[Re(CO)_3(bpy)Cl]$ (**1**), $[Re(CO)_3(bpy)(py)](CF_3SO_3)$ (**2**), $[Re(CO)_3(bpy)(CNx)](CF_3SO_3)$ (**3**), and $[Re(CO)(bpy)(CNx)_3](CF_3SO_3)$ (**4**), where bpy = 2,2′-bipyridine, py = pyridine, and CNx = 2,6-dimethylphenylisocyanide in their ground and lowest-lying triplet states. The ground-state optimized geometry for the cation of $[Re(CO)_3(bpy)(CNx)](CF_3SO_3)$ (**3**) results in a Re−C (CNx) bond length of 2.10 Å, a Re−C (CO) bond length trans to CNx of 2.01 Å, and a Re−C (CO) bond length cis to CNx of 1.96 Å which compares favorably to the single-crystal analysis of a Re−C (CNx) bond length of 2.074(4) Å, a Re−C (CO) bond length trans to CNx of 1.971(4) Å, and Re−C (CO) bond length cis to CNx of 1.932(4) Å. The majority of the singlet excited-state energies calculated using Time-dependent Density Functional Theory (TDDFT) and Conductor-like Polarizable Continuum Model (CPCM) are metal-ligand-to-ligand charge transfer (MLLCT) states and are in good agreement with the UV−vis spectral energies for the complexes in ethanol. The complexes exhibit emission both at room temperature and at 77 K except **4** which is only emissive at 77 K. The 77 K emission lifetimes range from 3.9 μs for **1** to 8.8 μs for **3**. The emissive lowest-lying triplet state is a ^{3}MLLCT state for complexes **1**−**3** but a triplet ligand-to-metal charge transfer (^{3}LMCT) state for complex **4**. The electronic, electrochemical, thermodynamic, HOMO−LUMO, and emitting-state energy gaps as well as the emission lifetimes increase in the order **1** < **2** < **3**. A ^3d−d excited- state, which is located above the ^{3}LMCT state, accounts for the loss of room-temperature emission for complex **4**.

Introduction

Density Functional Theory (DFT) is very useful for interpretation of electrochemical and spectroscopic results. A linear relationship between the HOMO−LUMO energy gap and the electrochemical redox potentials for a series of isoelectronic Ru(II) diimine complexes was reported from our laboratory.[1] DFT calculations on the ground and metal-

to-ligand charge transfer (MLCT) states of a series of Re(I) tricarbonyl complexes were used by others for the investigation of the excited-state geometries and electronic structures.[2−4] Time-dependent density functional theory (TDDFT) calculated MLCT states and UV−vis spectra correlations were also reported for Re(I) complexes containing the ligand azophenine.[4] The TDDFT method when used alone treats molecules in the gas phase; therefore, the method does not always give the right electronic excited-state energies in solution.[5,6a]

We have reported that combining the TDDFT with the conductor-like polarizable continuum model (CPCM) yields calculated singlet excited-state energies that correlate quite

---

* Corresponding author e-mail: paul.rillema@wichita.edu.
† Wichita State University.
‡ Bethany College.
§ Texas A & M University.

well with the UV−vis absorption energies of [Ru(bpy)₂-
(CNx)Cl]⁺ in a series of seven solvents of varied polarity.[6b]
According to other reports, the tandem use of TDDFT and
CPCM has produced dramatic changes in the energies and
the assignments of the singlet excited-states for Ru(II) and
Os(II) polypyridyl complexes.[7] It is the primary method used
in our study.

The synthesis, photochemistry, and computational studies
of 2,6-dimethylphenylisocyanide (CNx) complexes of Re(I)
and Ru(II) have been recently reported by our group.[8]
Generally, Re(I) diimine tricarbonyl complexes are *facial*,
MLCT emitters and have broad and structureless emission
bands which are sensitive to changes in the nature of the
environment.[9−11] Thus variations in the structure of the non-
carbonyl bidentate as well as the ancillary ligands could
produce considerable effects on luminescence energies,
lifetimes, and quantum yields. Here we report computational,
electronic absorption, and excited-state emission studies of
a series of Re(I) bipyridine complexes, [Re(CO)₃(bpy)Cl]
(**1**), [Re(CO)₃(bpy)(py)](CF₃SO₃) (**2**), [Re(CO)₃(bpy)(CNx)]-
(CF₃SO₃) (**3**), and [Re(CO)(bpy)(CNx)₃](CF₃SO₃) (**4**). The
photophysical properties of the two new complexes contain-
ing the CNx ligand, [Re(CO)₃(bpy)(CNx)]⁺, and [Re(CO)-
(bpy)(CNx)₃]⁺ are compared to similar properties of two
more conventional complexes, [Re(CO)₃(bpy)Cl] and [Re-
(CO)₃(bpy)(py)]⁺. The study is focused on the electronic
effect of the CNx ligand on the molecular geometry and
UV−vis and IR spectra of the Re(CO)₃(bpy) moiety using
computational and experimental methods.

Experimental Section

Materials. The ligand 2,6-dimethylphenylisocyanide was
purchased from Fluka. Re(CO)₅Cl, 2,2′-bipyridine, and
pyridine were purchased from Aldrich. Optima grade metha-
nol was purchased from Fischer Scientific, while acetonitrile
was purchased from Sigma-Aldrich. AAPER Alcohol and
Chemical Company was the source of absolute ethanol.
Ethanol and methanol were used in a 4:1 (v/v) mixture to
prepare solutions for the emission and emission lifetime
studies. Elemental analyses were obtained from Desert
Analytics Laboratory, Tucson, AZ.

Instrumentation and Physical Measurements. UV−vis
spectra were obtained using a Hewlett-Packard model 8452A
diode array spectrophotometer. The IR spectra were acquired
using a Nicolet Avatar 360 FT-IR spectrophotometer. Proton
NMR spectra were obtained using a Varian Mercury 300
FT-NMR spectrometer. An EG&G PAR model 263A po-
tentiostat/galvanostat was used to obtain the cyclic voltam-
mograms. The measurements were carried out in a typical
H-cell using a platinum disk working electrode, a platinum
wire counter electrode, and a Ag/AgCl reference electrode
in acetonitrile. The supporting electrolyte used was 0.1 M
tetrabutylammonium hexafluorophosphate (TBAH). Fer-
rocene was added for reference.

The sample preparation for emission studies involved
dissolving a small amount of sample (∼2 mg) in the
appropriate solvent, and the absorbance of the solution was
measured. The concentration of the solution was altered in
order to achieve an absorbance of about 0.10 at lowest energy

transition. Such a concentration provides enough material
for data acquisition but excludes self-quenching processes.
A 3−4 mL aliquot of the solution was then placed in a 10
mm diameter Suprasil (Heraeus) nonfluorescent quartz-tube
equipped with a tip-off manifold. The sample was then
freeze−pump−thaw degassed for at least three cycles (to
approximately 75 milliTorr) removing any gases from the
sample. The manifold was then closed, and the sample was
allowed to equilibrate at room temperature. The solvent
evaporation was assumed to be negligible; therefore, the
concentrations were assumed to remain constant throughout
this procedure. The corrected emission spectra were collected
using a Spex Tau3 Fluorometer.

The emission quantum yields were then calculated using
eq 1, where ϕ_x is the emission quantum yield of the sample
and ϕ_{std} is the emission quantum yield for the standard ([Ru-
(bpy)₃]²⁺), A_{std} and A_x represent the absorbance after degas-
sing the standard and the sample, respectively, while I_{std} and
I_x are the integrals of the emission envelope of the standard
and the sample, respectively.[12]

$$\phi_x = (A_{std}/A_x)(I_x/I_{std})\phi_{std} \tag{1}$$

The excited state lifetimes were determined by exciting
the sample at the lowest energy transition (usually MLCT)
using an OPOTEK optical parametric oscillator pumped by
a frequency tripled Continuum Surlite Nd:YAG laser run at
∼20 mJ/10 ns pulse. The oscilloscope control and data curve
fitting analysis was accomplished using the Origin 6.1
program by OriginLab Corporation. The excited state lifetime
experiments were conducted as previously published.[13]

X-ray Crystallography Data Collection. A Bausch and
Lomb 10× microscope was used to identify a suitable color-
less plate from a representative sample of crystals of [Re(bpy)-
(CO)₃(CNx)](PF₆) grown by slow evaporation of ethanol.
The crystal was coated in a cryogenic protectant (paratone)
and was then fixed to a loop which in turn was fashioned to
a copper mounting pin. The mounted crystal was then placed
in a cold nitrogen stream (Oxford) maintained at 110 K.

A BRUKER SMART 1000 X-ray three-circle diffracto-
meter was employed for crystal screening, unit cell deter-
mination, and data collection. The goniometer was controlled
using the SMART software suite, version 5.056 (Microsoft
NT operating system). The sample was optically centered
with the aid of a video camera such that no translations were
observed as the crystal was rotated through all positions. The
detector was set at 5.0 cm from the crystal sample (CCD-
PXL-KAF2, SMART 1000, 512 × 512 pixel). The X-ray
radiation employed was generated from a Mo sealed X-ray
tube (K_α = 0.70173 Å with a potential of 50 kV and a current
of 40 mA) and filtered with a graphite monochromator in
the parallel mode (175 mm collimator with 0.5 mm pinholes).

Dark currents were obtained for an exposure time of 30 s.
A rotation exposure was taken to determine crystal quality
and the X-ray beam intersection with the detector. The beam
intersection coordinates were compared to the configured co-
ordinates, and changes were made accordingly. The rotation
exposure indicated acceptable crystal quality, and the unit cell
determination was undertaken. Sixty data frames were taken
at widths of 0.3° with an exposure time of 10 s. Over 200 re-

Re(I) Bipyridyl Complexes

J. Chem. Theory Comput., Vol. 1, No. 1, 2005 **97**

Table 1. Crystal Data for [Re(bpy)(CO)$_3$(CNx)](PF$_6$), **3**

formula	C$_{22}$H$_{17}$F$_6$N$_3$O$_3$PRe
formula weight	702.56
crystal size, mm	0.30 × 0.20 × 0.05
crystal system	monoclinic
space group	P2(1)/n
a, Å	8.9203(18)
b, Å	12.925(3)
c, Å	21.104(4)
α, deg	90
β, deg	90.521(13)
γ, deg	90
V, Å^3	2433.2(8)
Z	4
density (calculated), g cm^{-1}	1.918
absorption coefficient, mm^{-1}	5.135
F(000)	1342
θ range for data collection, deg	1.85 to 28.30
index ranges	−11≤ h≤ 11, −17≤ k≤16, −20≤ l≤ 28
reflections collected	22815
independent reflections	5719 [R(int) = 0.0287]
completeness to θ	94.7%
max. and min. transmission	0.7833 and 0.3080
goodness-of-fit on F2	1.184
final R indices [I > 2σ(I)]	R1 = 0.0279, wR2 = 0.0748
R indices (all data)	R1 = 0.0319, wR2 = 0.0868
largest difference peak and hole, e Å^{-3}	2.435 and −0.681

flections were centered, and their positions were determined. These reflections were used in the auto-indexing procedure to determine the unit cell. A suitable cell was found and refined by nonlinear least squares and Bravais lattice procedures and reported here in Table 1. The unit cell was verified by examination of the *hkl* overlays on several frames of data, including zone photographs. No super-cell or erroneous reflections were observed.

After careful examination of the unit cell, a standard data collection procedure was initiated. This procedure consisted of a collection of one hemisphere of data using omega scans, involving the collection of 1201 0.3° frames at fixed angles for φ, 2θ, and χ (2θ = −28°, χ = 54.73°), while varying omega. Each frame was exposed for 30 s and contrasted against a 30 s dark current exposure. The total data collection was performed for duration of approximately 13 h at 110 K. No significant intensity fluctuations of equivalent reflections were observed.

After data collection, the crystal was measured carefully for size, morphology, and color. These measurements are reported in Table 1.

(1) Preparation of *fac*-[Re(bpy)(CO)$_3$Cl]. The synthesis of the complex was carried out following a previously published procedure.[14a,b] Yield 1.34 g (94%). Anal. Calcd for ReC$_{13}$H$_8$N$_2$O$_3$Cl: C, 33.81; H, 1.75; N, 6.07. Found: C, 34.00; H, 1.65; N, 6.04. IR (KBr pellet): 2022, 1890, 1653, 1600, 1559, 1471, 1444, 1314, 1245, 1070, 764, 732, 647, 536 cm^{-1}. ^{1}H NMR (DMSO): δ ppm 7.76 (dd, 2H, J = 0.9, 6.8 Hz), 8.35 (dd, 2H, J = 1.5, 7.7 Hz), 8.77 (d, 2H, J = 8.4 Hz), 9.02 (dd, 2H, J = 0.9, 5.5 Hz).

(2) Preparation of *fac*-[Re(bpy)(CO)$_3$(py)](CF$_3$SO$_3$). The synthesis of the complex was carried out following a previously published procedure.[14b,c] Yield 0.25 g (88%). Anal. Calcd for ReC$_{19}$H$_{13}$N$_3$O$_6$FS: C, 34.86; H, 2.00; N, 6.42. Found: C, 34.92; H, 1.82; N, 6.43. IR (KBr pellet): 2026, 1906, 1603, 1491, 1473, 1448, 1279, 1260, 1147, 1030, 776, 735, 700, 637, 573, 534 cm^{-1}. ^{1}H NMR (DMSO): δ ppm 7.42 (dd, 2H, J = 1.2, 7.2 Hz), 7.90 (dd, 2H, J = 1.2, 6.5 Hz), 7.95 (t, 1H, J = 7.8), 8.39 (m, 4H), 8.69 (d, 2H, J = 8.4 Hz), 9.31 (dd, 2H, J = 1.2, 5.7 Hz).

(3) Preparation of *fac*-[Re(bpy)(CO)$_3$(CNx)](CF$_3$SO$_3$). A 0.19 g sample of CNx (1.4 mmol) was added to a 100 mL round-bottomed flask containing 0.83 g of [Re(CO)$_3$-(bpy)(CF$_3$SO$_3$)] (1.4 mmol) in 50 mL of absolute ethanol. The mixture was refluxed for 6 h. The solvent was evaporated in vacuo until about 5 mL of the solution was left in the flask. The remaining solution was added dropwise into 100 mL of ether with constant stirring. The dark yellow precipitate was removed by filtration and dried in a vacuum. Yield: 1.00 g (98%). Anal. Calcd for ReC$_{23}$H$_{17}$N$_3$SF$_3$O$_6$: C, 39.10; H, 2.42; N, 5.95. Found: C, 40.40; H, 2.44; N, 5.68. IR (KBr pellet): 2173, 2036, 1955, 1603, 1473, 1443, 1279, 1224, 1152, 1033, 1025, 790, 638, 488 cm^{-1}. ^{1}H NMR (DMSO): δ ppm 1.98 (s, 6H), 7.17 (d, 2H, J = 7.8 Hz), 7.28 (t, 1H, J = 6.9 Hz), 7.85 (dd, 2H, J = 1.2, 6.8 Hz), 8.43 (dd, 2H, J = 1.5, 8.1 Hz), 8.86 (d, 2H, J = 7.8 Hz), 9.16 (d, 2H, J = 4.2 Hz).

(4) Preparation of *mer*-[Re(bpy)(CO)(CNx)$_3$](PF$_6$). A 0.10 g sample of mer-[Re(CNx)$_3$(CO)$_2$Cl][15] (0.15 mmol) was added to 0.05 g of AgPF$_6$ (0.20 mmol) and 0.03 g of 2,2′-bipyridine (0.18 mmol) in a 125 mL round-bottomed flask. About 75 mL of ethanol was added, and the solution was refluxed in the dark overnight. The solution was filtered to remove the solid AgCl, and the filtrate was evaporated to dryness. An orange solid was recovered, washed with ether, and dried under vacuum. Yield 0.11 g (81%). Anal. Calcd for ReC$_{38}$H$_{35}$N$_5$OPF$_6$: C, 50.21; H, 3.88; N, 7.71. Found: C, 50.41; H, 4.00; N, 7.90. IR (KBr pellet): 2072, 1885, 1658, 1590, 1468, 1439, 842, 774, 557, 491 cm^{-1}. ^{1}H NMR (DMSO): δ ppm 2.43 (s, 18H), 7.29 (m, 9H), 7.48 (dd, 2H, J = 0.9, 5.7 Hz), 7.97 (dd, 2H, J = 1.8, 8.1 Hz), 8.40 (dd, 2H, J = 0.9, 8.1 Hz), 8.70 (dd, 2H, J = 1.8, 4.5 Hz).

Results

Synthesis. The preparation of the complexes followed the scheme shown in Figure 1. Complexes **1** and **2** were prepared by modifying published procedures.[14] Complex **1** was synthesized by reacting [Re(CO)$_5$Cl] with bpy in ethanol, and it served as the starting material for complexes **2** and **3**. The chloro ligand was first removed from the coordination sphere by reaction of [Re(bpy)(CO)$_3$Cl] with AgCF$_3$SO$_3$ to precipitate AgCl generating the intermediate [Re(bpy)(CO)$_3$-(CF$_3$SO$_3$)]. Complex **2** was produced when py replaced CF$_3$SO$_3$$^-$ in the coordination sphere. Similarly, upon addition of CNx to a solution containing [Re(bpy)(CO)$_3$(CF$_3$SO$_3$)], complex **3** was obtained. The PF$_6$$^-$ salt of complex **3** was also prepared by first reducing the volume of the solvent using a rotary evaporator and then adding NH$_4$PF$_6$ to precipitate the product.
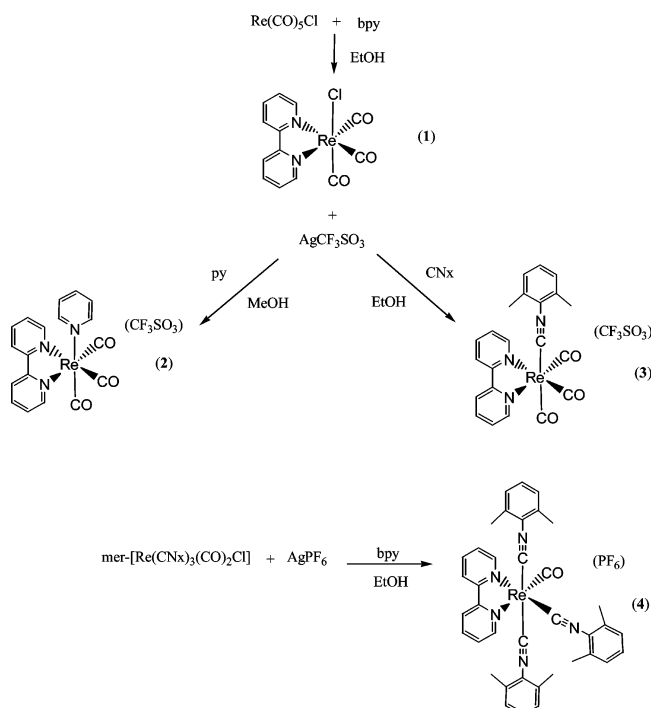
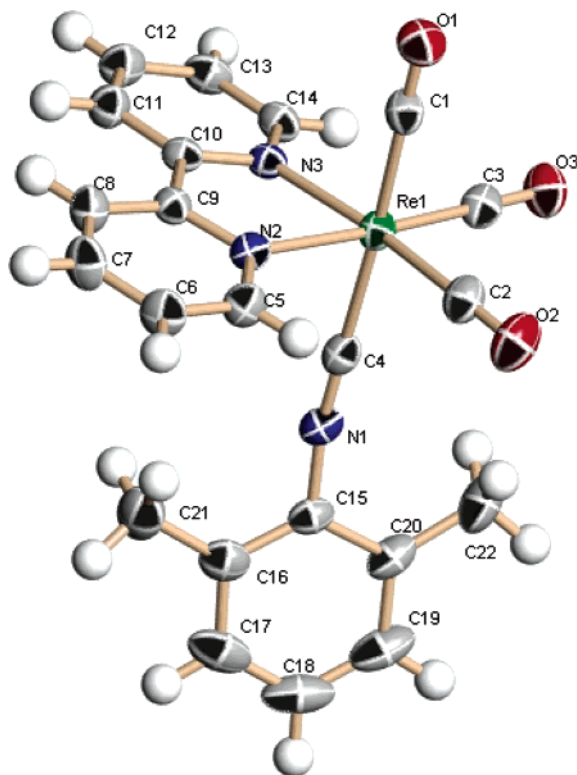**Figure 1.** Schematic diagram of the synthesis of the complexes.

Figure 2. ORTEP diagram of [Re(bpy)(CO)$_3$(CNx)]$^+$, **3**.

Complex **4** was prepared by a different route. The precursor complex, *mer*-[Re(CNx)$_3$(CO)$_2$Cl], was prepared using a modification of a previously published procedure.[15] This complex was refluxed with AgPF$_6$ and bpy in ethanol in the dark overnight to produce the desired product. The complexes were characterized by IR, ^{1}H NMR, and elemental analysis. The structure of the PF$_6^-$ salt of complex **3** was determined by X-ray crystallography.

Table 2. Selected Bond Length (Å) and Angles (deg) for [Re(bpy)(CO)$_3$(CNx)](PF$_6$), **3**

Re(1)−C(1)	1.971(4)	C(1)−Re(1)−C(4)	177.33(15)
Re(1)−C(2)	1.932(4)	C(2)−Re(1)−N(3)	173.56(15)
Re(1)−C(3)	1.927(4)	C(3)−Re(1)−N(2)	174.05(15)
Re(1)−C(4)	2.074(4)	O(1)−C(1)−Re(1)	178.5(4)
Re(1)−N(2)	2.171(3)	O(2)−C(2)−Re(1)	178.0(4)
Re(1)−N(3)	2.169(3)	O(3)−C(3)−Re(1)	177.5(4)
N(1)−C(4)	1.161(5)	N(1)−C(4)−Re(1)	175.8(3)
O(1)−C(1)	1.136(5)	C(4)−N(1)−C(15)	171.2(4)
O(2)−C(2)	1.151(5)		
O(3)−C(3)	1.147(5)		

X-ray Crystal Structure Determination of *fac*-[Re-(CO)$_3$(bpy)(CNx)](PF$_6$) (3). The structure of **3** was determined by X-ray crystallography and is shown in the ORTEP diagram of Figure 2. The crystal data are listed in Table 1, while selected bond distances and angles for the complex are given in Table 2.

The complex adopted a distorted octahedral geometry with the equatorial plane defined by the bipyridine ligand and two carbonyl groups trans to it and the axial ligands defined as a carbonyl group with a CNx ligand opposite it. The angles of the trans ligands at the metal center were 177.33(15)° for C(1)−Re(1)−C(4), 173.56(15)° for C(2)−Re(1)−N(3), and 174.05(15)° for C(3)−Re(1)−N(2). The Re−N bond lengths were similar within experimental error, 2.17 ± 0.01 Å, as well as the Re−C (CO) bond distances, 1.93 ± 0.02 Å, in the equatorial positions. However, the Re−C (CO) bond length of CO trans to the CNx ligand was considerably longer by ∼0.04 Å compared to the other two Re−C (CO) bond distances. The longest Re−C bond distance was 2.074(4) Å to the CNx ligand.

Electronic Absorption Studies. The electronic absorption properties of the complexes were studied at room temperature in 4:1 ethanol/methanol as solvent. Molar absorption coefficients (ϵ) were determined from Beer's Law plots using at least five dilution points. The probable assignments of these bands were made on the basis of the documented optical transitions of similar Re(I) complexes[9,16,17] and the computational assignment of the singlet excited-states (vide infra). The results are listed in Table 3.

The lowest energy transition of the complexes was assigned as metal−ligand-to-ligand charge transfer (MLLCT), while those at higher energies were assigned as the intraligand $\pi \rightarrow \pi^*$ transitions. The MLLCT absorption peaks of the series occurred in the following order: **4** (26 200 cm^{-1}) < **1** (26 900 cm^{-1}) < **3** (27 000 cm^{-1}) < **2** (28 600 cm^{-1}). In addition to the optical transition for **3** located at 27 000 cm^{-1}, another one was found at 30 300 cm^{-1}. It is important to note that since the MLLCT band occurs as a broad shoulder, the exact position of the band maximum as well as the extinction coefficient were subject to error.

The intraligand $\pi \rightarrow \pi^*$ transitions were located in the UV region of the spectrum. As expected, the molar absorptivities of the electronic transitions associated with the CNx ligand[8b] (33 000 and 42 000 cm^{-1}) increased as the number of coordinated CNx ligands increased from one in **3** to three in **4**.

Electrochemical Studies. The redox potentials of the series of complexes were determined using cyclic voltam-

Re(I) Bipyridyl Complexes

J. Chem. Theory Comput., Vol. 1, No. 1, 2005 **99**

Table 3. Experimental[a] Electronic Transitions and Calculated[b,c] Excited State Energies of Re(I) Complexes

complex	E_{exp}, $\times 10^3$ cm^{-1}, ϵ (M^{-1} cm^{-1})	E_{calc}, $\times 10^3$ cm^{-1}	assignment
[Re(bpy)(CO)$_3$Cl]	26.9 (3900)	25.0	MLLCT
	34.2 (15 200)	34.1	LC ($\pi \rightarrow \pi^*$)
	41.7 (16 400) (s)[d]		LC ($\pi \rightarrow \pi^*$)
[Re(bpy)(CO)$_3$(py)](CF$_3$SO$_3$)	28.6 (4400)	27.4	MLLCT
	31.2 (13 300)		MLLCT
	32.7 (12 300)	32.8	MLLCT[e]
	37.9 (18 800)	37.4	MLLCT[e]
	40.0 (19 200)	39.7	MLLCT
[Re(bpy)(CO)$_3$(CNx)](CF$_3$SO$_3$)	27.0 (2300) (s)[d]	26.8	MLLCT
	31.6 (22 700)	31.5	MLLCT
	32.9 (21 800)	32.6	MLLCT
	38.5 (49 300)	37.9	MLLCT[e]
[Re(bpy)(CO)(CNx)$_3$](PF$_6$)	26.2 (7000) (s)[d]	26.7	MLLCT
	29.1 (22 000) (s)[d]	29.0	MLLCT
	32.7 (53 000) (s)[d]	32.8	MLLCT
	34.0 (59 000)	34.3	MLLCT
	42.0 (45 000)		LC ($\pi \rightarrow \pi^*$)

[a] In 4:1 (v/v) ethanol:methanol. [b] In ethanol. [c] Only singlet excited-states with $f > 0.05$ are considered. [d] s = shoulder. [e] Mixed state.

Table 4. Electrochemical Properties of the Complexes in CH$_3$CN at Room Temperature

complex	$E_{1/2 (ox)}$, V[a]	$E_{1/2 (red)}$, V[a]
[Re(bpy)(CO)$_3$Cl][b]	1.32[d]	-1.35
[Re(bpy)(CO)$_3$(py)](CF$_3$SO$_3$)	1.78[d]	-1.18[b]
[Re(bpy)(CO)$_3$(CNx)](CF$_3$SO$_3$)	1.99[d]	-1.22
[Re(bpy)(CO)(CNx)$_3$](PF$_6$)	1.30[e]	
[Ru(bpy)$_3$]$^{2+}$[(c)]	1.27[f]	-1.31
		-1.50
		-1.77

[a] Potential in volts vs SSCE (scan rate = 250 mV/s). [b] Data from ref 14. [c] Data from ref 13. [d] Irreversible oxidation wave. [e] Quasi-reversible oxidation wave. [f] RuIII/II redox couple.

metry. The electrochemical properties of the complexes are listed in Table 4. Irreversible oxidation waves attributed to the Re(I) → Re(II) process increased in potential in the order **1** < **2** < **3** for [Re(CO)$_3$(bpy)Cl] (**1**), [Re(CO)$_3$(bpy)(py)]$^+$ (**2**), and [Re(CO)$_3$(bpy)(CNx)]$^+$ (**3**). The single reduction observed for **1**−**3** was attributed to the reduction of the bpy ligand.

The electrochemical behavior of [Re(CO)(bpy)(CNx)$_3$]$^+$ (**4**) differed from the others. It underwent a quasi-reversible oxidation ($\Delta E_p = 0.09$ V) at 1.30 V attributed to the Re(II/I) couple. Further, a reduction normally associated with coordinated bpy was absent. The oxidation of **4** was shifted to a lower potential compared to the other three complexes.

Emission Properties and Excited-State Lifetimes. The emission properties and excited-state lifetimes of the complexes were studied both at room temperature and at 77 K. The results are given in Table 5. Complexes **1**−**3** were emissive both at room temperature and at 77 K. Complex **4** however was nonemissive at room-temperature but was highly emissive at 77 K.

The emission lifetimes (τ_{em}) increased in the order **1** < **2** < **3** both at room temperature and at 77 K as Cl in **1** was replaced with py in **2** and CNx in **3**. The emission quantum yield (ϕ_{em}) also increased from 0.0052 for **1** to 0.10 for **2** and 0.27 for **3**. It is worthy to note that ϕ_{em} determined at room temperature for complex **3** was more than three times higher than ϕ_{em} of the standard complex [Ru(bpy)$_3$]$^{2+}$ under the same experimental conditions. The ϕ_{em} of complex **2** was also slightly higher than the standard under the same conditions. At 77 K, complex **4** produced an intense, structureless emission peak centered at 20 600 cm^{-1}.

Computational Section

The singlet ground-state geometries of the complexes **1**−**4** were optimized in the gas phase using the B3LYP[18] functional of the Gaussian '03[19] program package. The Stuttgart-Dresden (SDD) ECP[20] was used for the Re core potentials. The {(8s7p6d)/[6s5p3d]}-GTO was applied for the valence shell of Re together with the all-electron 6-311G*

Table 5. Calculated ^{3}MLLCT State Energies[a] and Emission Properties of the Complexes at 77 K and Room Temperature[b,f]

complexes	E_{calc}	E_{exp} 77 K	E_{exp} RT	τ_{em}, μs 77 K	τ_{em}, μs RT	φ_{em}[d] RT
[Re(bpy)(CO)$_3$Cl][c]	20.6	19.2	16.8	3.9	0.037	0.0052
[Re(bpy)(CO)$_3$(py)](CF$_3$SO$_3$)[c]	21.4	20.2	18.0	5.4	0.33	0.10
[Re(bpy) (CO)$_3$(CNx)](CF$_3$SO$_3$)	21.9	22.2	19.3	8.8	1.22	0.27
		20.9				
		19.6 (s)[e]				
		18.0 (s)[e]				
[Re(bpy)(CO)(CNx)$_3$](PF$_6$)	21.4	20.6		6.3		

[a] In ethanol. [b] In 4:1 ethanol/methanol. [c] Emission properties were also reported in CH$_2$Cl$_2$ in refs 9 and 14. [d] Relative to [Ru(bpy)$_3$]$^{2+}$ (ref 13). [e] (s) = shoulder. [f] Energies in $\times 10^3$ cm^{-1}.

Table 6. Selected Geometry Parameters of **3** Based on Calculated Singlet Ground and Lowest-Lying Triplet State Geometries and X-ray Crystallography

source	Re−N₂, Å	Re−C₄, Å	Re−C₁, Å	Re−C₂, Å	N₁−C₄, Å	C₁−O₁, Å	C₂−O₂, Å	Re−C₄−N₁, deg	Re−C₁−O₁, deg	C₄−N₁−C₁₅, deg
X-ray	2.171(3)	2.074(4)	1.971(4)	1.932(4)	1.161(5)	1.136(5)	1.151(5)	175.8(3)	178.5(4)	171.2(4)
singlet	2.23	2.10	2.01	1.96	1.17	1.14	1.15	177.8	179.6	178.4
triplet	2.16	2.09	2.06	1.99	1.17	1.13	1.14	179.1	179.9	178.7

Table 7. Calculated Triplet Excited-States of Complexes **1−4** in Ethanol Based on the Lowest-Lying Triplet State Geometry[a]

state	f	$\psi_o \rightarrow \psi_v$	type	E_{VER}
		Complex 1		
1	0.00	H-2 → H (1.0)	Re_d, CO → Re_d, Cl	22.9
2	0.00	H-3 → H (1.0)	bpy → Re_d, Cl	25.8
3	0.01	H-1 → H (1.0)	Re_d, Cl → Re_d, Cl	27.0
4	0.02	L → L+2 (0.8)	bpy → bpy	32.6
		L → L+4 (0.6)	bpy → del	
		Complex 2		
1	0.00	H-2 → H (1.0)	Re_d, CO → Re_d, CO	24.8
2	0.00	H-3 → H (1.0)	bpy → Re_d, CO	25.5
3	0.02	H-1 → H (1.0)	Re_d, CO → Re_d, CO	26.7
4	0.00	L → L+1 (1.0)	bpy → py	32.1
		Complex 3		
1	0.00	H-2 → H (1.0)	Re_d, CO → Re_d, CNx	25.8
2	0.00	H-4 → H (1.0)	bpy → Re_d, CNx	26.2
3	0.04	H-1 → H (0.9)	Re_d → Re_d, CNx	26.5
4	0.00	H-3 → H (1.0)	CNx → Re_d, CNx	31.9
		Complex 4		
1	0.00	H-3 → H (1.0)	CNx → Re_d, CNx	21.4
2	0.00	H-2 → H (0.8)	Re_d, CNx → Re_d, CNx	22.0
		H-1 → H (0.6)	Re_d, CNx → Re_d, CNx	
3	0.00	L → L+1 (1.0)	bpy → CNx	24.2
4	0.01	H-1 → H (0.8)	Re_d, CNx → Re_d, CNx	26.0
		H-2 → H (0.5)	Re_d, CNx → Re_d, CNx	

[a] E_{VER} is the energy of the vertical transition in $\times 10^3$ cm⁻¹, f is the oscillator strength, and ψ_o and ψ_v are the occupied and the virtual orbitals that define the transition. The transition type is determined based on the change in the spatial distribution from occupied to virtual orbital. The absolute value of the transition coefficient for each transition is given in parentheses. H = HOMO, L = LUMO, and del = delocalized. (See text for calculation details.)

basis set[21] for Cl, O, N, C, and H atoms. Selected parameters of the optimized geometry of complex **3** are presented in

Table 6. The optimized geometries of the complexes are listed in Supporting Information Table S1.

Nonequilibrium TDDFT[22]/CPCM[23] calculations were employed to produce a number of singlet excited-states[24] of complexes **1−4** in ethanol based on the singlet ground-state geometry optimized in the gas phase.[25] The output contained information for the excited-state energies and oscillator strengths (f) and a list of the excitations that give rise to each excited state, the orbitals involved as well as the wave function coefficients of the excitations. The singlet excited-states of the four complexes are presented in Figure 3 as vertical bars with height equal to the extinction coefficient calculated from the oscillator strength.[5,6]

The lowest-lying triplet state geometries of the four complexes were calculated using unrestricted B3LYP in the gas phase. The spin contamination from states of higher multiplicity was low. The value of $\langle S^2 \rangle$ was 2.010 for **1**, 2.012 for **2**, 2.018 for **3**, and 2.017 for **4**. The energies of the lowest-lying triplet states were higher than these of the corresponding ground states by 20 600 cm⁻¹ for **1**, 21 400 cm⁻¹ for **2**, 21 900 cm⁻¹ for **3**, and 16 800 cm⁻¹ for **4** (Table 7 and Figure 4). The lowest-lying triplet states were ³MLLCT states and featured single HOMO and LUMO occupancy.

A number of triplet excited-states were computed based on the ³MLLCT state geometry for the four complexes. The four low-lying triplet excited-states are listed in Table 7 and shown in Figure 3, even if the f value is low. These excited states were used for the interpretation of the temperature-dependent emission properties of the complexes.

Vibrational analysis was performed using B3LYP for the ground-state optimized geometries of the four complexes. The frequencies of the most intense vibrations are presented in Table 8.

Table 8. Calculated and Experimental Vibrational IR Frequencies (cm⁻¹) for the Four Complexes[a]

	1		2		3		4		
	calc.	exp.	calc.	exp.	calc.	exp.	calc.	exp.	assignment
					2173	2173	2084	2072[c]	a[b]
	2037	2022	2061	2026	2065	2036	1950	1885	b[b]
	1964	sh	1989	sh	2013	sh			b[b]
	1939	1890	1977	1906	1992	1955			b[b]
			1608	1603	1597	1603	1603	1590	c[b]
	1466	1471	1484	1448	1467	1473	1468	1468	d[b]
	757	764	765	776	763	790	761	774	e[b]
	634	647	629	637	623	638	589	557	f[b]
					496	488	488	491	g[b]

[a] The calculated values were factored by 0.975. [b] a = CN stretch, b = CO stretch, c = CNx or py ring breathing modes, d = bpy ring breathing modes, e = out-of-plane H (bpy) vibrations, f = symmetric CO bending, and g = CNx vibrations. [c] Calculated vibrational frequencies at 2154 and 2099 cm⁻¹ correspond to shoulders near the experimental peak at 2072 cm⁻¹.
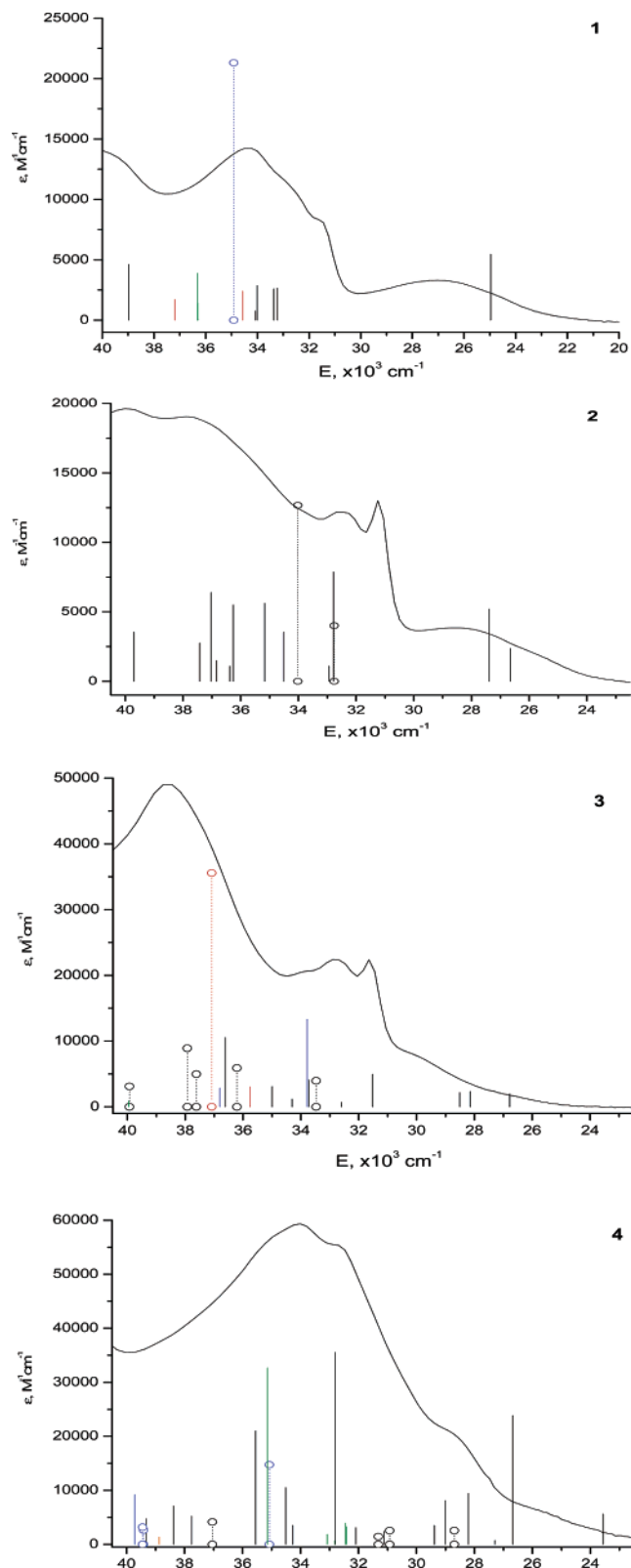
Figure 3. Experimental absorption spectra of **1**−**4** and calculated singlet excited-states. The excited states are shown as vertical bars with height equal to the extinction coefficient.[5a] Black = MLLCT, green = LLCT, blue = $\pi \rightarrow \pi^*$, red = MCDCT, orange = Re$_d$, CNx $\rightarrow$ Re$_s$ and ($\bigcirc$·······$\bigcirc$) = mixed excited-state.

Discussion

X-ray Structure. As noted in the results section, [Re(CO)$_3$-(bpy)(CNx)]$^+$ (**3**) adopted a distorted octahedral geometry.
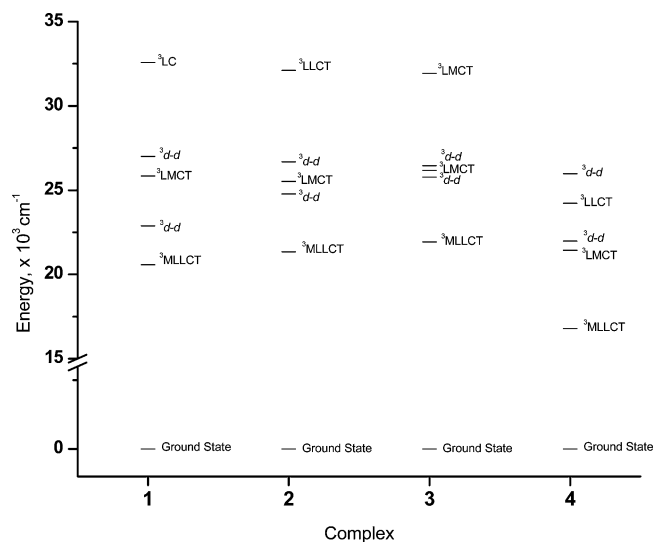
Figure 4. Triplet excited-state energy diagram for complexes **1**−**4**.

The increase in Re−C (CO) bond distance of 0.04 Å compared to the other two Re−C (CO) bond distances is a result of the trans effect resulting from the strong σ donating character of the CNx ligand to the metal center. The bond elongation of CO trans to the CNx ligands of 0.04 Å was analogous to that reported for the [Ru(bpy)$_2$(CNx)$_2$](PF$_6$)$_2$ by our group where the Ru−N (bpy) trans to CNx was 0.03 Å longer than for Ru−N (bpy) cis to CNx.[8a]

In a related X-ray crystallographic study, the Re−C (L) distance in *cis*-[ReCl(CO)$_3$L$_2$] (L = 2,6-diisopropyl-4-acetyleno-phenylisocyanide)[26] was 2.092(5) Å, or 0.02 Å longer than the Re−C (CNx) distance found for [Re(CO)$_3$-(bpy)(CNx)](PF$_6$). The Re−C (CO trans to L) distance of 1.973(6) Å was the same as Re−C (CO trans to CNx) in this report. However for Re−C with CNx trans to CNx, the bond distance for [Re(CNx)$_5$Cl] was only 2.019(7) Å[8b] compared to 2.074(4) Å for [Re(CO)$_3$(bpy)(CNx)]$^+$. The Re−C (CNx) distance was longer by 0.12 Å than the Ru−C (CNx) distance in [Ru(bpy)$_2$(CNx)$_2$](PF$_6$)$_2$.[8a] This may be due to the larger ionic radius of Re(I).

Molecular Orbitals. The molecular orbital energy diagram for the four complexes in ethanol is shown in Figure 5. The HOMO, HOMO-1, and HOMO-2 of complexes **1**−**4** contained 50% or higher Re$_d$ character. The remaining contribution was from the nonimine ligands. Additionally, for complex **1**, the HOMO and HOMO-1 contained equal contributions (∼20% for each) from the CO and Cl moieties, whereas HOMO-2 contained 23.5% CO but less than 1% Cl character. The HOMO, HOMO-1, and HOMO-2 for complex **2** contained ∼20% CO character and negligible imine ligand contributions. For complex **4**, the HOMO, HOMO-1, and HOMO-2 contained more than 23% CNx ligand contributions while the CO contributions were low. The HOMO of complex **3** contained ∼32% CNx ligand contribution, whereas the HOMO-1 and HOMO-2 contained 18% or higher CO character (the CNx ligand contribution was less than 7%). The LUMOs contained 80% or higher bpy ligand π^* character (Figure 6). The LUMOs+1 were located on the bpy and py ligands for complexes **1** and **2**,
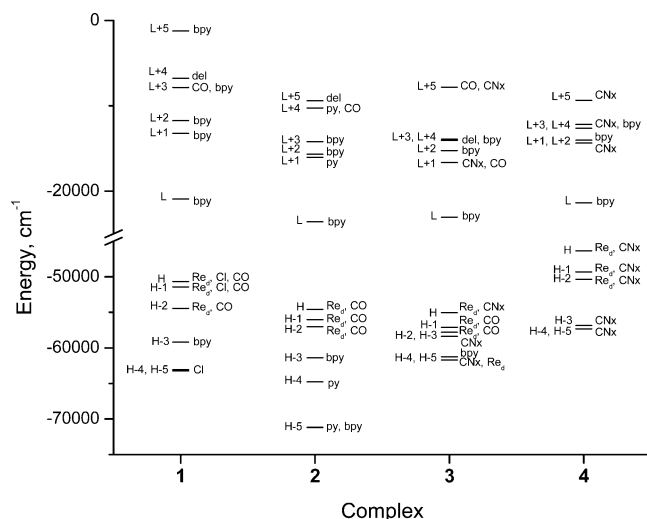
Figure 5. Molecular orbital energy diagram for six occupied and six virtual frontier orbitals of **1**−**4** in the singlet ground state in ethanol.
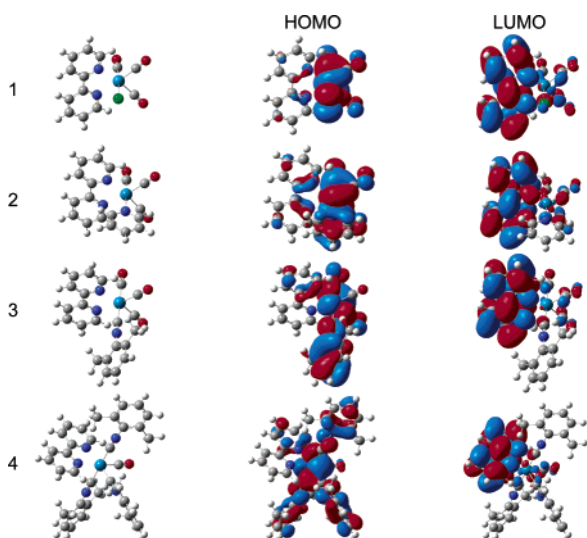

Figure 6. HOMO and LUMO schematic diagrams for complexes **1**−**4**.

respectively, and on the CNx ligands for complexes **3** and **4**. The percent orbital contributions are listed in Supporting Information Table S2.

The schematic diagrams of the HOMO and the LUMO for the four complexes are shown in Figure 6. The HOMOs contained more than 50% Re_d character and the remaining contributions were almost evenly distributed among the nonimine ligands, whereas the LUMOs were on the bpy ligand. The HOMO−LUMO energy difference increased from 29 800 cm^{-1} for complex **1**, to 31 000 cm^{-1} for **2**, and 32 000 cm^{-1} for **3**. The HOMO−LUMO energy gap for complex **4** was only 25 000 cm^{-1}.

Geometry Optimization of 3. Selected parameters of the optimized geometry of complex **3** in the singlet ground and lowest-lying triplet states are listed in Table 6, next to the results of the X-ray structure determination. The singlet ground-state bond lengths and bond angles presented are in general agreement with the experimental values. The Re−N distances were overestimated by ∼0.05 Å and the Re−C

(CO and CNx) distances by ∼0.03−0.04 Å. The $C_4−N_1−C_{15}$ angle was 178.4° in comparison to the 171.2° found experimentally. The elongation of the Re−C (CO trans to CNx) bond relative to Re−C (CO cis to CNx) was confirmed computationally. It was due to the electron-donating effect of the isocyanide ligand (vide infra). The deviation of the experimental value from 180° could be a result of crystal packing effects. These results obtained with one of the largest basis sets appear satisfactory despite the shortcomings associated with the calculation of the metal−ligand bond lengths using B3LYP functional.[5,6a]

The geometry of complex **3** in the ^{3}MLLCT state was slightly different from the ground-state geometry. The differences listed in Table 6 can be interpreted using the molecular orbital schematic diagram shown in Figure 6. The Re−N_2 distance decreased from 2.23 to 2.16 Å in the triplet relative to the singlet ground state. This bond shortening could be due to the mixing between the Re dπ HOMO and the bpy π* LUMO in the lowest-lying triplet state as reported for *fac*-[Re(bpy)(CO)$_3$(4-ethylpyridine)]$^+$.[2a] The Re−C_1 and Re−C_2 distances increased by 0.05 Å and 0.03 Å, respectively. The bonding character of the HOMO with respect to the Re−C (CO) bonds could account for these bond elongations in the triplet state. The bonding and antibonding character was determined by visual examination of the phases of the molecular orbital for each diagram. The phases are related to the spatial distributions of alpha (α) and beta (β) electron densities[27] shown in red and blue colors, respectively.

Mulliken Charges. Mulliken charges were calculated for the singlet ground-state geometry, and the solvent effect of ethanol was accounted for using CPCM. The changes in the Mulliken charge of the metal atom can be used for the evaluation of the electron-donating power of the ligands.[8a] The Re charge lowering can be expressed as follows: $Re^{calc} = Re^{1-\Sigma nL}$, where n is the number of coordinated atoms from ligand L. The relative electron-donating power of CNx was 0.08 as determined from the 0.54 charge on Re[8b] for [Re(CNx)$_6$]$^+$ using the following mathematical relationship, $Re^{0.54} \sim Re^{1-6\times0.08}$. Analogously, the electron-donating power of CO was determined to be 0.11 based on a residual charge of 0.34 on Re[28] for [Re(CO)$_6$]$^+$. For [Re(CO)$_3$(bpy)(CNx)] the donating power of each coordinated N atom was determined to be −0.05 from the following: $Re^{0.81} \sim Re^{1-3\times0.11-3(-0.05)}$. The electron donating power of the ligands for Re(I) can be arranged as follows CO > CNx > N. When these electron donating powers are used to calculate the predicted Re charge produced for complexes **3** and **4**, the values obtained were in good agreement with the DFT computed values. For complexes **3** and **4** the above approach produced $Re^{1-3\times0.11-1\times0.08-2\times(-0.05)} = Re^{0.69}$ and $Re^{1-1\times0.11-3\times0.08-2\times(-0.05)} = Re^{0.75}$ compared to 0.67 and 0.73, respectively, from DFT. The Re charge in complex **1** was 0.56. However, Mulliken charge analysis of the donating power of the chloro ligand for complex **1** was not performed due to concerns of properly accounting for the negative charge on the chloro ligand by the CPCM method.

The donating power of CNx and N (imine) is greater for Ru(II) (CNx = 0.32; N = 0.1)[8a] than for Re(I) (CNx = 0.08; N = −0.05), but in both cases the contribution of CNx >
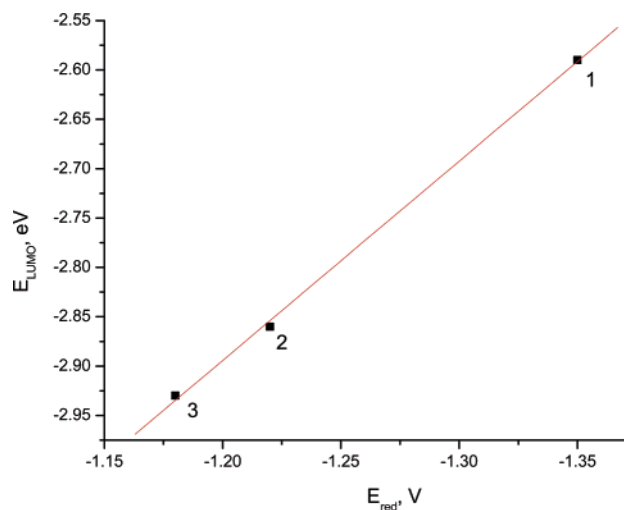
Re(I) Bipyridyl Complexes

J. Chem. Theory Comput., Vol. 1, No. 1, 2005 **103**

Figure 7. Linear dependence of $E_{1/2(red)}$ and the LUMO energies for complexes **1**–**3**.

N. Also the contribution of each to Re(I) is smaller than to Ru(II). Perhaps the differences are due to the initial charges of the complexes, but more examples are needed to unravel the trends.

Electrochemical Behavior. The electronic effects of the CNx ligand were evident in the electrochemical results as listed in Table 4. The redox potentials of importance are those derived from the processes involving the HOMOs which contained primarily Re $d\pi$ orbitals and the LUMOs which contained the π^* orbital located on the bpy ligand. Hence, oxidation involves the removal of an electron from Re (HOMO) and reduction involves the addition of an electron to the bpy π^* orbital (LUMO).

The reduction potentials were assigned based on the energies and spatial distributions of the LUMO (Figure 5). The potential for the single reduction of the bpy ligand increased from −1.35 V for **1** to −1.22 V for **3** and −1.18 V for **2**. The reduction potentials of complexes **1**–**3** were linearly dependent on the DFT calculated LUMO energies as shown in Figure 7. The slope of the line was −2.0 (±0.1) compared to −2.32 reported for a series of 10 isoelectronic Ru(II) diimine complexes.[1]

The oxidation potentials however, which varied considerably across the series, were all irreversible and increased from **1** to **3**. The energy gap between the HOMO and the LUMO increased in the order **1** < **2** < **3**. The potential differences (E_{ox} − E_{red}) follow the same order as the room-temperature emission maxima. The results indicated the parallel relationship between the thermodynamic and electronic energy gaps.[29,30] The fact that **3** has the highest energy gap compared to **1** and **2** indicated the strong influence of the CNx ligand on the system.

Singlet Excited-States and Electronic Absorption Spectra. The singlet excited-states of complexes **1**–**4** with $f >$ 0.01 are shown in Figure 3 as vertical bars with height equal to the extinction coefficient. The bars are presented in colors that correspond to the type of singlet excited-state as follows: black = MLLCT, green = LLCT, blue = $\pi \rightarrow \pi^*$, orange = Re$_d$,CNx $\rightarrow$ Re$_s$, and red = MCDCT (metal-to-complex-delocalized charge transfer). These assignments were made based on the major contributing excitation. The

singlet excited-states had contributions from several excitations. For those presented with solid bars there was one major contributing excitation (with a transition coefficient for the major excitation being higher than the transition coefficient of the other excitations by more than 0.2). For some singlet excited-states, however, there was more than one contributing excitation with high transition coefficients. Singlet excited-states that contained contributions from several excitations with transition coefficients that were within 0.2 of the major excitation transition coefficient are assigned as mixed singlet excited-states and are presented with the vertical bars symbolized as ○·······○.

The excited states of complex **1** were mostly of MMLCT type. All of the MLLCT states were associated with transitions that originated from the HOMO, HOMO-1, and HOMO-2 that contained Re$_d$, Cl, and CO contributions. The excited state at 34 900 cm^{-1} with the highest ϵ involved equal contributions from bpy $\pi \rightarrow \pi^*$ and an MLLCT state. Two degenerate Cl $\rightarrow$ bpy excited-states were computed at 36 300 cm^{-1}. The singlet excited-states of complex **2** were assigned as Re$_d$,CO $\rightarrow$ bpy and Re$_d$,CO $\rightarrow$ py states, or MLLCT states. Excited states 4 and 7 (shown with the notation ○·······○ in Figure 3) contained significant bpy $\pi \rightarrow \pi^*$ contributions. The majority of the singlet excited-states of complex **3** were MLLCT states. In addition, there were two $\pi \rightarrow \pi^*$ states, one involving the bpy ligand and the other involving the CNx ligand. The singlet excited-state at 39 900 cm^{-1} was due to three excitations—a CNx ligand $\pi \rightarrow \pi^*$, MMLCT, and a CNx $\rightarrow$ bpy with transition coefficients of 0.4, 0.3, and 0.3, respectively. This state was labeled as $\pi \rightarrow \pi^*$ according to the assignment of the major excitation and is shown in Figure 3 as a blue vertical line symbolized as ○·······○. For complex **4**, the singlet excited-states below 32 000 cm^{-1} were mainly of MLLCT character. The singlet excited-state at 35 200 cm^{-1} was assigned as LLCT (CNx $\rightarrow$ bpy). Two CNx $\pi \rightarrow \pi^*$ states were calculated at 39 400 and 39 700 cm^{-1}. The higher CNx ligand contribution to the frontier molecular orbitals and the smaller HOMO−LUMO gap for complex **4** compared to **1**–**3** resulted in an increase in the number of singlet excited states calculated in the energy range 28 000−32 000 cm^{-1}. These excited states correlated well with the experimental peak broadening and the merging of the LC and MLLCT peaks in complex **4**. The singlet excited-states are listed in Supporting Information Table S3.

The calculated singlet excited-state energies correlated well with the experimental UV−vis peaks in the same solvent (Figure 3 and Table 3). For complex **1**, the MLLCT singlet excited-state at 25 000 cm^{-1} is 1900 cm^{-1} lower in energy relative to the position of the broad UV−vis peak at 26 900 cm^{-1}, whereas the bpy $\pi \rightarrow \pi^*$ excited-state at 34 100 cm^{-1} is 100 cm^{-1} lower than the most intense experimental peak at 34 200 cm^{-1}. For complex **2** the MLLCT excited-state at 27 400 cm^{-1} was 1200 cm^{-1} lower in energy compared to the UV−vis peak at 28 600 cm^{-1}. The mixed excited-states at 32 800 and 37 400 cm^{-1} were within 500 cm^{-1} from the UV−vis peaks at 32 700 and 37 900 cm^{-1}, respectively. These states were assigned as MLLCT but contained significant $\pi \rightarrow \pi^*$ character. For complex **4**, the singlet excited-states of 32 800 cm^{-1} and 34 300 cm^{-1} were blue-

shifted by 100 cm^{-1} and 300 cm^{-1} relative to the experimental peaks at 32 700 and 34 000 cm^{-1}, respectively. The excited states were of MLLCT type. For complexes **2**−**4**, the agreement between the calculated and experimental data was remarkable. The experimental peaks at energies higher than 40 000 cm^{-1} were assigned as $\pi \rightarrow \pi^*$ states according to the conventional assignment. Simulation of the singlet excited-states into Gaussian line shapes and subsequent integration, following a procedure previously reported[5a] (not shown), did not correlate well with the UV−vis spectrum curvature. The use of the TDDFT/CPCM method is known to produce optical energies in good agreement with the experimental absorption spectra. The oscillator strengths calculated using TDDFT/CPCM method were higher than both the experimental values determined in the respective solvent and the calculated values in the gas phase for a series of ruthenium-(II) polypyridyl complexes containing CNx ligand.[6b,8a] In another study, the f values computed in 2-methyltetrahydrofurane solution using the TDDFT/PCM method were also significantly higher than the experimental values in the same solvent and the calculated values in the gas phase.[31]

Triplet Excited-States. Four triplet excited-states for each of the complexes **1**−**4** were computed in ethanol based on the ^{3}MLLCT geometry and are listed in Table 7. The major excitations in these states had transition coefficients higher than 0.8. The three lowest-lying triplet excited-states for complexes **1**−**3** involved excitations to the rhenium and nonimine ligand centered HOMO (Figure 6). These states were pure, with the transition coefficients of the major excitations of 1.0. Excited state 4 for complexes **1** and **2** involved excitations from the LUMO (bpy) to LUMO+2 (bpy) and LUMO+1 (py), respectively. In complex **4** each of the triplet excited-states 2 and 4 involved two excitations of the same type.

The relative energies of the triplet excited-states are presented in the schematic diagram in Figure 4. The excited states that involved occupied and virtual molecular orbitals with more than 50% Re contribution were assigned as ^3d−d states, whereas states that involved ligand-to-metal charge-transfer excitations, like states 2 for complexes **1**−**3**, were assigned as ^{3}LMCT states. The energies of the ^{3}MLLCT states increase from 20 600 cm^{-1} for **1**, 21 400 cm^{-1} for **2**, and 21 900 cm^{-1} for **3** following the same trend as the experimental emission energies of 19 200 cm^{-1} for **1**, 20 200 cm^{-1} for **2**, and 22 200 cm^{-1} for **3** at 77 K. Above the ^{3}MLLCT states were ^3d−d states and ^{3}LMCT states for complexes **1**−**3**. The ^{3}MLLCT state of complex **4** was only 16 800 cm^{-1} above the ground state, and the ^{3}LMCT state at 21 400 cm^{-1} was only 200 cm^{-1} lower than the experimental emission energy at 77 K. The ^{3}LMCT is then assigned as the emitting state for complex **4**. The thermal population of the ^3d−d state at 22 000 cm^{-1} accounts for the loss of room-temperature emission of complex **4**.

The ^3d−d and ^{3}LLCT states were obtained via single electron vertical excitations from the ^{3}MLCT states and the excited-state energies reported were not the minima.[32] The ^3d−d transitions are symmetry forbidden[33] and have very low oscillator strengths (Table 7). The role of the ^3d−d states in quenching room-temperature emission is discussed in the succeeding section.

Recent study suggests that the addition of diffuse functions to double-ζ basis sets can improve the effectiveness of DFT for the calculations of reaction and conformation energies of butadiene and 1,2-ethanediol.[34a] In a TDDFT/PCM study the 6-311++G** basis set is utilized for a more complete description of the mixing between the valence and Rydberg excite states of acrolein.[34b] Further studies on the effects of the addition of diffuse functions to double and triple-ζ basis sets for the calculation of excited-state energies are needed and have the potential of improving the results presented here.

Vibrational Analysis. The vibrational frequencies for the four complexes were calculated, factored[35] by 0.975, and listed in Table 8. The most distinct and intense calculated frequencies were correlated with the experimental results. The C≡N and C=O stretching modes were among the most pronounced peaks. Excellent agreement was obtained between the calculated and the experimental values of the C≡N stretching frequencies for complexes **3** and **4**. For complex **4**, there were three C≡N stretching modes calculated but only the one at 2072 cm^{-1} was resolved experimentally. The calculated frequencies at 2154 and 2099 cm^{-1} corresponded to the shoulders on both sides of the experimental peak at 2072 cm^{-1}. Three C=O stretching frequencies were calculated for each of the complexes **1**−**4** and correlated with the experimental values. The assignment of the three C=O frequencies for each of the complexes **1**−**3** was limited by the experimental resolution. Both the experimental and the calculated C=O stretching modes shifted to higher frequencies in the order **1** < **2** < **3**. The higher vibrational frequency of **3** was anticipated based on the electron-donating power of the CNx ligand. The calculated values were higher than the experimental by 30 cm^{-1}−75 cm^{-1}. The calculated ring breathing and symmetric C=O bending modes correlated well with the experimental values. In the low energy range of the spectrum an intense vibration was located. According to the computational results this involved the vibration of the CNx ligand with respect to the rest of the complex. The vibrational frequency of CNx for **3** was computed at 496 cm^{-1}, compared to the experimental value of 488 cm^{-1}. For complex **4**, three CNx specific vibrations were expected, but only one was resolved experimentally. The coordinated CNx ligand vibrations occurred ~20 cm^{-1} lower in frequency than the corresponding modes in [Ru(bpy)$_2$(CNx)Cl]$^+$, [Ru(bpy)$_2$-(CNx)(py)]$^{2+}$, and [Ru(bpy)$_2$(CNx)$_2$]$^{2+}$.[8a] This shift is likely due to the heavier Re atom.

Emission Properties and Excited-State Lifetimes. The room-temperature emission spectra of complexes **1**−**3** compared to [Ru(bpy)$_3$]$^{2+}$ are shown in Figure 8A. The 77 K emission spectra of complexes **1**−**4** are presented in Figure 8B. Complex **4** was nonemissive at room temperature. The emission maxima of the complexes at 77 K are blue-shifted compared to that at room temperature.

Figure 9 shows a model diagram that will aid in discussing the observed emission properties and excited-state lifetimes of the complexes in the series. It shows the three states involved—ground state, ^{3}MLCT, and ^{3}LC (triplet ligand-centered state) both at room temperature and at 77 K. In this case, the ^{3}MLCT state is taken to be essentially temperature dependent. Hence, the energy gap between the
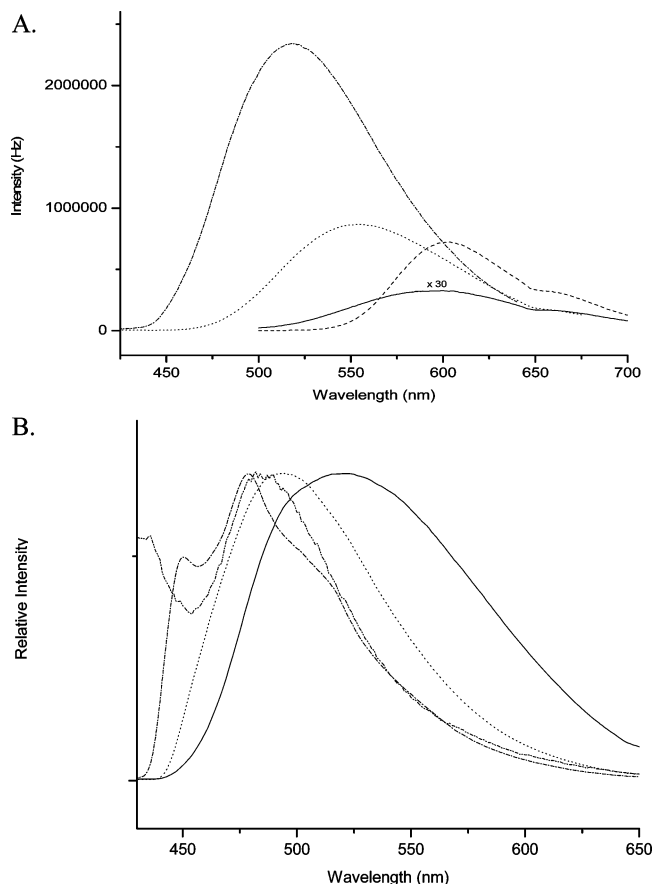
A.

B.

Figure 8. Emission spectra of complexes **1** (—), **2** (···), **3** (- · -), and [Ru(bpy)$_3$]$^{2+}$ (- - -) at room temperature (A) and **1** (—), **2** (···), **3** (- · -), and **4** (- ·· -) at 77 K (B) in 4:1 (v/v) ethanol: methanol.
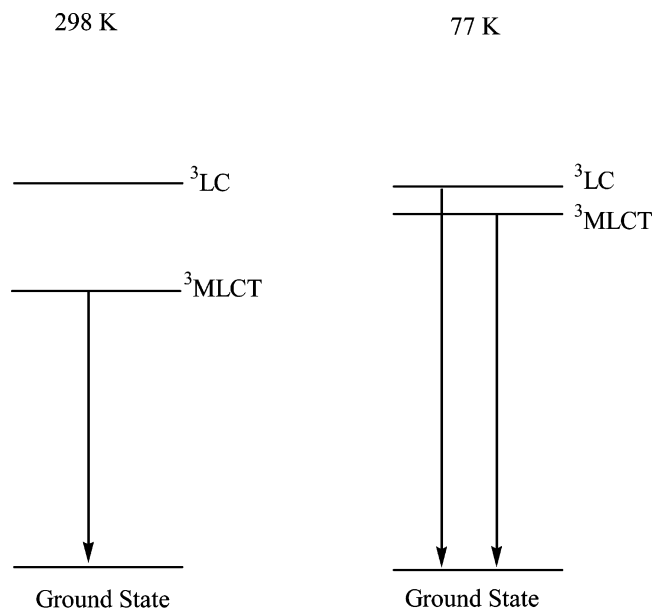
298 K   77 K

Figure 9. Energy level diagram showing the emitting state of the complexes in the series.

emitting triplet state at room temperature is smaller than at 77 K resulting in the observed blue shift of the emission maxima at 77 K relative to room temperature. At room temperature, the emitting state is the ^{3}MLCT, which is equilibrated with respect to the solvent environment and

geometry of the complex. The reorientation of the solvent cage is fast compared to the rate of deactivation of the emitting state. The trend of increasing emission energies and excited-state lifetimes in the order **3** > **2** > **1** is in accord with the energy gap law. The thermodynamic and the electronic energy gaps increase parallel to each other in the above order as has been previously reported.[17]

Conclusion

Four Re(I) bipyridyl complexes were investigated using spectroscopic methods and DFT calculations. The results were correlated and revealed the following: (1) The electronic, electrochemical, thermodynamic, HOMO−LUMO, and emitting state energy gaps as well as the emission lifetimes and ^{3}MLLCT energies increased in the order **1** < **2** < **3**. (2) The electron-donating power of the CNx ligand was evaluated, and its effect on the computed optimized geometry parameters, singlet excited states, and C=O vibrational frequencies was correlated with the experimental results from X-ray crystallography and UV−vis and IR spectroscopies. (3) The three complexes (**1**−**3**) were emissive both at room temperature and at 77 K. (4) The complexes showed reversible reduction but irreversible oxidation waves. (5) The LUMO energies were linearly dependent on the reduction potentials of complexes **1**−**3**. (6) Complex **4** was nonemissive at room temperature but showed intense emission at 77 K with a lifetime of 6.3 μs which is longer than 5.4 μs for complex **2** but shorter than the 8.8 μs for **3**. A low-lying ^3d−d state was responsible for the loss of room-temperature emission in **4**. The complex showed a reversible oxidation but no reduction wave.

Supporting Information Available: Crystallographic data for [Re(bpy)(CO)$_3$(CNx)](PF$_6$) in CIF format, the optimized geometries (Table S1), the percent orbital contributions (Table S2), and the calculated singlet excited-state energies of the four complexes (Table S3). This material is available free of charge via the Internet at http://pubs.acs.org.

References

(1) Stoyanov, S. R.; Villegas, J. M.; Rillema, D. P. *Inorg. Chem.* **2002**, *41*, 2941.

(2) Dattelbaum, D. M.; Martin, R. L.; Schoonover, J. R.; Meyer, T. J. *J. Phys. Chem. A* **2004**, *108*, 3518−3526. (b) Dattelbaum, D. M.; Omberg, K. M.; Hay, J. P.; Gebhart, N. L.; Martin, R. L.; Schoonover, J. R.; Meyer, T. J. *J. Phys. Chem. A* **2004**, *108*, 3527−3536.

(3) Yang, L.; Ren, A.-M.; Feng, J.-K.; Liu, X.-J.; Ma, Y.-G.; Zhang, M.; Liu, X.-D.; Shen, J.-C.; Zhang, H.-X. *J. Phys. Chem. A* **2004**, *108*, 6797−6808. (b) Dyer, J.; Blau, W. J.; Coates, C. G.; Creely, C. M.; Gavey, J. D.; George, M. W.; Grills, D. C.; Hudson, S.; Kelly, J. M.; Matousek, P.; McGarvey, J. J.; McMaster, J.; Parker, A. W.; Towrie, M.; Weinstein, J. A. *Photochem. Photobiol. Sci.* **2003**, *2*, 542−554.

(4) Frantz, S.; Rall, J.; Hartenbach, I.; Schleid, T.; Zalis, S. Kaim, W. *Chem.-A Eur. J.* **2004**, *10*, 149−154.

(5) Monat, J. E.; Rodriguez, J. H.; McCusker, J. K. *J. Phys. Chem. A* **2002**, *106*, 7399. (b) Rodrigues, J. H.; Wheeler, D. E.; McCusker, J. K. *J. Am. Chem. Soc.* **1998**, *120*, 12051.

(6) Stoyanov, S. R.; Villegas, J. M.; Rillema, D. P. *Inorg. Chem.* **2003**, *42*, 7852. (b) Stoyanov, S. R.; Villegas, J. M.; Rillema, D. P. *Inorg. Chem. Commun.* **2004**, *7*, 838−841.

(7) Guillemoles, J.-F.; Barone, V.; Joubert, L.; Adamo, C. *J. Phys. Chem. A* **2002**, *106*, 11345.

(8) Villegas, J. M.; Stoyanov, S. R.; Wei, H.; Lockyear, L. L.; Reibenspies, J.; Rillema, D. P. *Inorg. Chem.* **2004**, *43*, 6383−6396. (b) Villegas, J. M.; Stoyanov, S. R.; Reibenspies, J.; Rillema, D. P. *Organomet.* **2004**, submitted.

(9) Wrighton, M.; Morse, D. L. *J. Am. Chem. Soc.* **1974**, *96*, 998. (b) Giordano, P. J.; Wrighton, M. S. *J. Am. Chem. Soc.* **1979**, *101*, 2888.

(10) Lees, A. *J. Chem. Rev.* **1987**, *87*, 711. (b) Giordano, P. J.; Fredericks, S. M.; Wrighton, M. S.; Morse, D. L. *J. Am. Chem. Soc.* **1978**, *100*, 2257.

(11) Leasure, R. M.; Sacksteder, L.; Nesselrodt, D.; Reitz, G. A.; Demas, J. N.; DeGraff, B. A. *Inorg. Chem.* **1991**, *30*, 3722.

(12) Jovanovic, B.; Manojlovic-Muir, Lj.; Muir, K. W. *J. Chem. Soc., Dalton Trans.* **1972**, 1178.

(13) Villegas, J. M.; Stoyanov, S. R.; Rillema, D. P. *Inorg. Chem.* **2002**, *41*, 6688.

(14) Giordano, P. J.; Fredericks, S. M.; Morse, D. L.; Wrighton, M. S. *J. Am. Chem. Soc.* **1978**, *100*, 2257. (b). Caspar, J. V.; Meyer, T. J. *J. Phys. Chem.* **1983**, *87*, 952−957. (c) Luong, J. C. Ph.D. Thesis, Massachusetts Institute of Technology, 1981.

(15) Treichel, P. M.; Williams, J. P. *J. Organomet. Chem.* **1977**, *135*, 39−51.

(16) Wrighton, M. S.; Geoffroy, G. L. *Organometallic Photochemistry*; Academic Press: New York, 1979; Chapter 2. (b) Luong, J. C.; Nadjo, L.; Wrighton, M. S. *J. Am. Chem. Soc.* **1978**, *100*, 5790.

(17) Wallace, L.; Rillema, D. P. *Inorg. Chem.* **1993**, *32*, 3836−3843.

(18) Becke, A. D. *Phys. Rev. A* **1988**, *38*, 3098. (b) Becke, A. D. *J. Chem. Phys.* **1993**, *98*, 5648. (c) Lee, C.; Yang, W.; Parr, R. G. *Phys. Rev. B* **1988**, *37*, 785. (d) Vosko, S. H.; Wilk, L.; Nusair, M. *Can. J. Phys.* **1980**, *58*, 1200.

(19) Frisch, M. J.; Trucks, G. W.; Schlegel, H. B.; Scuseria, G. E.; Robb, M. A.; Cheeseman, J. R.; Montgomery, J. A., Jr.; Vreven, T.; Kudin, K. N.; Burant, J. C.; Millam, J. M.; Iyengar, S. S.; Tomasi, J.; Barone, V.; Mennucci, B.; Cossi, M.; Scalmani, G.; Rega, N.; Petersson, G. A.; Nakatsuji, H.; Hada, M.; Ehara, M.; Toyota, K.; Fukuda, R.; Hasegawa, J.; Ishida, M.; Nakajima, T.; Honda, Y.; Kitao, O.; Nakai, H.; Klene, M.; Li, X.; Knox, J. E.; Hratchian, H. P.; Cross, J. B.; Adamo, C.; Jaramillo, J.; Gomperts, R.; Stratmann, R. E.; Yazyev, O.; Austin, A. J.; Cammi, R.; Pomelli, C.; Ochterski, J. W.; Ayala, P. Y.; Morokuma, K.; Voth, G. A.; Salvador, P.; Dannenberg, J. J.; Zakrzewski, V. G.; Dapprich, S.; Daniels, A. D.; Strain, M. C.; Farkas, O.; Malick, D. K.; Rabuck, A. D.; Raghavachari, K.; Foresman, J. B.; Ortiz, J. V.; Cui, Q.; Baboul, A. G.; Clifford, S.; Cioslowski, J.; Stefanov, B. B.; Liu, G.; Liashenko, A.; Piskorz, P.; Komaromi, I.; Martin, R. L.; Fox, D. J.; Keith, T.; Al-Laham, M. A.; Peng, C. Y.; Nanayakkara, A.; Challacombe, M.; Gill, P. M. W.; Johnson, B.; Chen, W.; Wong, M. W.; Gonzalez, C.; Pople, J. A. *Gaussian 03*, revision B.03; Gaussian, Inc.: Pittsburgh, PA, 2003.

(20) Andrae, D.; Hauessermann, U.; Dolg, M.; Stoll, H.; Preuss, H. *Theor. Chim. Acta* **1990**, *77*, 123.

(21) McLean, A. D.; Chandler, G. S. *J. Chem. Phys.* **1980**, *72*, 5639. (b) Krishnan, R.; Binkley, J. S.; Seeger, R.; Pople, J. A. *J. Chem. Phys.* **1980**, *72*, 650.

(22) Stratmann, R. E.; Scuseria, G. E.; Frisch, M. J. *J. Chem. Phys* **1998**, *109*, 8218. (b) Bauernschmitt, R.; Ahlrichs, R. *Chem. Phys. Lett.* **1996**, *256*, 454. (c) Casida, M. E.; Jamorski, C.; Casida, K. C.; Salahub, D. R. *J. Chem. Phys.* **1998**, *108*, 4439.

(23) Cossi, M.; Barone, V. *J. Chem. Phys.* **2001**, *115*, 4708. (b) Barone, V.; Cossi, M. *J. Phys. Chem. A* **1998**, *102*, 1995. (c) Cossi, M.; Rega, N.; Scalmani, G.; Barone, V. *J. Comput. Chem.* **2003**, *24*, 669.

(24) The CPCM is designed to account for the bulk physical properties of the solvent. It does not account for specific solvent−solute interactions. The TDDFT is known to perform well for the computing of charge transfer excited-states between closely spaced moieties.

(25) Geometry optimization in solvents was not achieved. Partial optimizations (change in distance of less than 0.001 Å and change in angles of less than 0.01°) followed by TDDFT/CPCM calculation produced excited-state energies that were not in better agreement with the experimental excited-state energies than the excited-state energies based on the gas-phase optimized geometry.

(26) Yang, L.; Cheung, K.-K.; Mayr, A. *J. Organomet. Chem.* **1999**, *585*, 26−34.

(27) Foresman, J. B.; Frisch, Æ. *Exploring Chemistry with Electronic Structure methods*, 2nd ed.; Gaussian Inc.: Pittsburgh, PA, 1996; pp 206, 215.

(28) The geometry of $[Re(CO)_6]^+$ was optimized using the procedure described in the Computational section and is available in Supporting Information Table S1.

(29) Juris, A.; Campagna, S.; Bidd, I.; Lehn, J. M.; Zeissel, R. *Inorg. Chem.* **1988**, *27*, 4007.

(30) Della Ciana, L.; Dressick, W. J.; Sandrini, D.; Maestri, M.; Ciano, M. *Inorg. Chem.* **1990**, *29*, 2792.

(31) Wan, J.; Ren, Y.; Wu, J.; Xu, X. *J. Phys. Chem. A* **2004**, *43*, 9453−9460.

(32) The triplet excited-states were calculated based on the lowest-lying triplet state geometry because according to Kasha's rule this state would be the emitting state. Thus the triplet excited-states were determined based on the most stable triplet geometry. Triplet excited-states calculated based on the singlet ground-state geometry are multiplicity forbidden ($f = 0$).

(33) Drago, R. S. *Physical Methods for Chemist*, 2nd ed.; Saunders College Publishing: Orlando, Florida, 1992; p 123.

(34) Lynch, B. J.; Zhao, Y.; Truhlar, D. G. *J. Phys. Chem. A* **2003**, *107*, 1384−1388. (b) Aquilante, F.; Barone, V.; Roos, B. *J. Chem. Phys.* **2003**, *119*, 12323−12333.

(35) The correction factor is within the range reported for correction of B3LYP computed vibrational frequencies for positive transition metal complex ions as outlined in the following: Zhou, M.; Andrews, L.; Bauschlicher, C. W., Jr. *Chem. Rev.* **2001**, *101*, 1931.